Analysis of Deep Pulse-Coupled Neural Networks for diagnosis of non-small cell lung cancers disease using CTScans

V.Deepa[1], Dr.S.K,B Sangeetha[2]
Department of Computer Science and Engineering, Srm Institute of Science and Technology, Vadapalani,Chennai, India.

Abstract:

The Non-Small Cell Lung Cancer (NSCLC) is the most common type of lung cancer, comprising about 85% of cases, often treated with surgery, chemotherapy, and radiation. This includes advanced imaging, biopsy, and molecular testing, along with tailored treatments like surgery, radiation, chemotherapy, targeted therapy, and immunotherapy. Continuous monitoring, supportive care, and research for new therapies are crucial. It is necessary to detect NSCLC, so many techniques are implemented. But the existing methods have lot of disadvantages such as over fitting, quality control and limited data availability. To overcome the aforementioned problem, Deep Pulse-Coupled Neural Networks with Multi-axis vision transformer using Bowerbird Optimization Algorithm (DPCNN-MAVT-BOA) is proposed for accurately detecting NSCLC. In this input image is taken from LC25000, TCGA and GEO Dataset for the purpose of denoising and picture enhancement Anisotropic Gaussian side windows Guided Filtering (AGSWGF) is proposed. Following that pre-processed images are segmented using Patch-Based Cross-Layer Non-Local Attenuation based MobileNet (PCLNL-MobileNet). After that feature extraction and classification are done using Deep Pulse-Coupled Neural Networks with Multi-axis vision transformer (DPCNN-MAVT) and optimization are done using Bowerbird Optimization Algorithm (BOA) for detecting tumor and normal conditions of the NSCLC. The efficiency of the proposed DPCNN-MAVT-BOA is analyzed using 3 datasets and attains 99.78% accuracy, 97.29% recall and attains better results compared with the existing methods. The establishment of an accurate and automated approach for classifying different forms of NSCLC may be greatly aided by these output.

Key words: *Non-small cell Lung cancer detection, Anisotropic Gaussian side windows Guided Filtering, Cascaded Residual Deep Capsule Group Neural Networks, Bowerbird Optimization Algorithm*

1. Introduction:

Parenchymal cell proliferation that is aberrant and unchecked is the root cause of NSCLC. One of the most prevalent forms of cancer cases is lung cancer. Both the prevalence and death rate from cancer are increasing every day [1]. Lung cancer can be categorized as small cell lung cancer (SCLC) or non-small cell lung cancer (NSCLC) based on histological characteristics [2]. Lung cancer, the most common form of non-small cell lung cancer (NSCLC), is linked to the highest death rate globally. Small cell lung cancer (15%) and non-small cell lung cancer (85%) are the two categories. The current treatment for those with advanced SqCC is chemotherapy because molecular medications for lung ADC usually don't work against lung SqCC. Precision medicine depends on quick and non-invasive techniques to differentiate lung SqCC from lung ADC. A thorough examination of tumor heterogeneity has been demonstrated by recent developments in radiomics and machine learning (ML). Deep learning (DL) technology is a desirable alternative since it can automatically identify essential illness traits from medical photos [3-5]. A deadly disease, lung cancer claims the lives of around 1.8 million people each year and accounts for 1.4 million new cases. About 85% of all instances of lung cancer are classified as non-small cell lung cancer (NSCLC), which is further subdivided into three subtypes: Lung Adenocarcinoma (LUAD), Lung Squamous Cell carcinoma (LUSC), and Lung Large Cell carcinoma (LULC). About 90% of the histological subtypes of NSCLC are accounted for by LUAD and LUSC. Early diagnosis is essential for enhancing therapeutic interventions and raising survival rates. Although they have limitations in detecting lung masses, diagnostic Imaging methods like magnetic resonance imaging (MR), PET/CT, and computed tomography (CT) are recommended. CT, particularly low-dose CT, enables 3D thoracic vision and is sensitive to small, calcified lung masses [6-9]. Lung cancer is the second most common type of cancer worldwide. Incidence and mortality rates for cancer were 2.1 million and 1.8 million worldwide in 2018, respectively, accounting for almost 20% of all cancer fatalities. The five-year survival rate prediction for the early stage ranges from 68 to 92%, and for the extremely late stage, it drops sharply below the 10% threshold at 42%. Thus, to increase a patient's chances of survival and lower treatment costs, lung cancer must be detected and treated early [10-12]. Phase III Non-small cell lung cancer (NSCLC) accounts for thirty percent of cases and is the primary cause of cancer-related deaths globally. With an anticipated 5-year survival range of 13% to 36%, despite improvements in treatment, stage III NSCLC still has a dismal overall prognosis. By avoiding local failures and distant metastases, neoadjuvant Concurrent Chemo Radio Therapy (CCRT) followed by surgery has an improved

overall result. Using 18F-FDG PET/CT imaging, prognostic variables for non-small cell lung cancer have been postulated; however, typical PET parameters only indicate the tumor's total glucose metabolism. Clinical diagnosis and treatment response in There is a strong correlation between non-small cell lung cancer and radiomics, which could be used to extract tumor phenotypic traits. This study evaluates the predictive impact of radiomic features on overall survival in patients with stage III [13–14].This retrospective study aimed to ascertain the predictive usefulness of the latter by comparing the number of resected metastatic lymph nodes (MLN) from non-small cell lung cancer (NSCLC) using the Pathologic Nodal (PN) category as the current staging approach [15].

Novelty and Contribution

- The Anisotropic Gaussian Side Windows Guided Filtering (AGSWGF) goal is to reduce noise in the input images and improve the quality of the input images.
- Patch-Based Cross-Layer Non-Local Attenuation based MobileNet (PCLNL-MobileNet) intends to remove unneeded parts in order to aid the algorithm in making the best diagnosis possible.
- The objective of employing feature extraction and classification using Deep Pulse-Coupled Neural Networks with Multi-axis vision transformer (DPCNN-MAVT) it is helpful to improve the efficiency of feature extraction and also used for classify the input images. This approach aims to enhance the NSCLC detection and classification of input images, and its parameters are optimizes using a novel BOA.

The section 2 reviews the literature; Section 3 suggests a technique; Section 4 presents the results and comments; and Section 5 concludes with future work.

2. Literature Survey:

In 2023, Hamed et.al [16] has introduced Lung cancer is the second most common cause of mortality worldwide and one of the worst types of the disease. Accurate and early identification of lung cancer histology is necessary to improve survival rates. Artificial intelligence (AI) can find more cancer cases faster and at a lower cost by automating the diagnosing process. The ability of a CNN model to distinguish between images of benign and malignant lung cancer from digital pathology is evaluated in this work. The accuracy of the model ranged from 99.9% to 100%, which reduced processing time.

In 2023 Halder et.al [17] has introduced the MorphAttnNet, a novel deep learning framework that classifies lung cancer subtypes based on image morphology. The framework accurately captures the morphological changes of lung cancer subtypes through the application of morphological procedures and convolution. The system achieved high sensitivity, specificity, average accuracy, precision, and f1-score of 98.33%, 97.76%, 98.96%, 99.12%, and 98.72%, respectively, using the LC25000 dataset that is open to the public. Additionally, the system performed better than current cutting-edge technologies.

In 2024 Noaman et.al [18] has introduced the artificial intelligence (AI) and histological image analysis, this study explores early cancer diagnosis. To increase classification accuracy, DenseNet201 is combined with color histogram approaches. Support Vector Machines and K-Nearest Neighbors are two of the eight machine learning algorithms that are evaluated in this study. 99.683% accuracy rate on LC25000 and 94.808% accuracy rate on BreakHis are attained by the model. The results show how AI can be used for histopathology analysis and offer recommendations for future developments and practical applications.

In 2023 Cao et.al [19] has introduced the two main challenges in classifying non-small cell lung cancer (NSCLC) are the presence of vast redundant regions and scattered feature regions in pathology imaging. A fine-grained categorization network called the Progressive Jigsaw and Graph Convolutional Network (PJGC-Net) is proposed to overcome these issues. The network consists of two modules: the GCN-Based multi-scale puzzle generating module for fine-grained learning and the Jigsaw supervised progressive training module for removing superfluous sections. Experimental results show that the strategy outperforms other methods of categorization.

In 2024 Zheng et.al [20] has introduced the research is to find a possible molecular target for lung treatment adenocarcinoma that is connected to cancer-associated fibroblasts. Hub gene screening, confirmation of COL11A1's differential expression and survival, and assessment of the relationship between Weighted Gene Co-expression Network Analysis (WGCN) and immune checkpoint genes in human malignancies were all conducted using the Cancer Genome Atlas lung adenocarcinoma dataset.

In 2023 Sultana et.al [21] has introduced finds gene biomarkers for NSCLC prognosis and diagnosis using scRNA-seq data. There were 158 DEGs found, 48 of which were up-regulated and 110 of which were down-regulated. Twelve important genes were found and their prognostic, expression, and diagnostic potential assessed.

In 2023 Dwivedi et.al [22] has introduced the novel deep learning framework powered by AI to find biomarkers for many non-small cell lung cancer subtypes (NSCLC). An auto encoder, a Feed-Forward Neural Network, and a biomarker finding module make up the framework. It was discovered that the biomarkers were significant for classifying NSCLC subtypes, with Multilayer Perceptron attaining a 95.74% accuracy rate. Of the 52 biomarkers, 45 have been published in prior research, while seven are still being investigated for targeted treatment of lung cancer.

In 2024 Wang et.al [23] has introduced a radiomic model that uses CT features to predict tumor mutational burden (TMB) level to detect the immunotherapy level in lung cancer. Utilizing 3D-Slicer software, the model was created. It was then validated using ROC curves and outside datasets, and its suitability for clinical use was evaluated by decision curve analysis.

In 2023 Guo et.al [24] has introduced the Pericentriolar Material 1 (PCM1)'s function in cancer was investigated in this study by examining 411 lung adenocarcinoma (LUAD) and control samples. It was discovered that, maybe as a result of its antagonistic effects on RHOC, higher levels of PCM1 expression were linked to better survival prospects. It was discovered that PCM1 was mostly expressed in membrane and cytoplasmic components. According to the study, treating patients with elevated PCM1 levels may benefit from the use of targeted and chemotherapeutic medicines.

In 2024 Verma et.al [25] has introduced the gene-disease connections and patient gene expression data are combined, biomedical knowledge bases (KBs) can improve medical diagnostic decision support systems. Using these real world datsets the repiratory viral infections can be detected.When it came to detecting infections within 72 hours, LOADDx achieved an average accuracy of 92.66%, while SCADDx achieved an accuracy of up to 100%. These algorithms beat other machine learning techniques. The different techniques and methods used in existing ones is mentioned in Table 1

In 2024 chen et.al [26] has introduced To find putative biomarkers for non-small cell lung cancer (NSCLC) with R software and machine learning methods. Findings indicated that specific siRNAs reduced the expression of GDF10, NCKAP5, and RTKN2 in A549 and H1975 cells, indicating a potential involvement of resting NK cells, Tregs, and activated dendritic cells in NSCLC.

Table1: Summary of the existing methods

Reference Number	Methods	Advantages	Disadvantages
[16]	CNN	High accuracy and comprehensive performance metrics. Combines conventional and deep learning techniques.	May require large annotated datasets, potential over fitting
[17]	MorphAttnNet	High performance metrics, effective morphological feature extraction	Complex model, computationally intensive
[18]	K-NN	High classification accuracy, versatile across different datasets	Potentially high computational complexity, reliance on color histogram
[19]	PJGC-Net	Effective in handling redundant and scattered feature regions	Complexity of the jigsaw and GCN modules, potential over fitting
[20]	WGCN	Provides molecular targets for therapy, uses comprehensive dataset analysis	Requires validation in clinical settings, potential for false positives.
[21]	PPIN	Identifies potential biomarkers, uses single-cell RNA sequencing data	Requires further validation, potential complexity in data interpretation

[22]	FFNN	High accuracy, identifies significant biomarkers	Potentially high computational complexity, reliance on prior research for biomarker validation
[23]	3D Slicer	Useful for predicting treatment response, validated with decision curve analysis	Requires extensive image processing, potential for over fitting

Problem Statement:

Non-Small Cell Lung Cancer (NSCLC) is significant because it presents an opportunity to identify the shortcomings of existing treatments through the development of a highly accurate, dependable, and efficient method. Using datasets such as LC25000, TCGA, and GEO, the proposed Deep Pulse-Coupled Neural Networks with Multi-axis Vision Transformer optimized by Bowerbird Algorithm (DPCNN-MAVT-BOA) seeks to achieve improved detection accuracy, recall, and performance by reducing errors and improving generalization.

3 Proposed Methodology

In this section, the input data is taken from three dataset such as LC25000 dataset, TCGA dataset and GEO datasets. Then these data are pre-processed using Anisotropic Gaussian Side Windows Guided Filtering (AGSWGF) method. Following that, NSCLC is segmented using the Patch-Based Cross-Layer Non-Local Attenuation based mobilenet (PCLNL-MobileNet) method. Then feature extraction and classifications are done using Deep Pulse-Coupled Neural Networks with Multi-axis vision transformer (DPCNN-MAVT) method and optimized with Bowerbird Optimization Algorithm (BOA). DPCNN-MAVT-BOA is used for detecting the normal and tumor conditions of NSCLC. Figure 1 shows the Process flow diagram of the proposed DPCNN-MAVT-BOA.

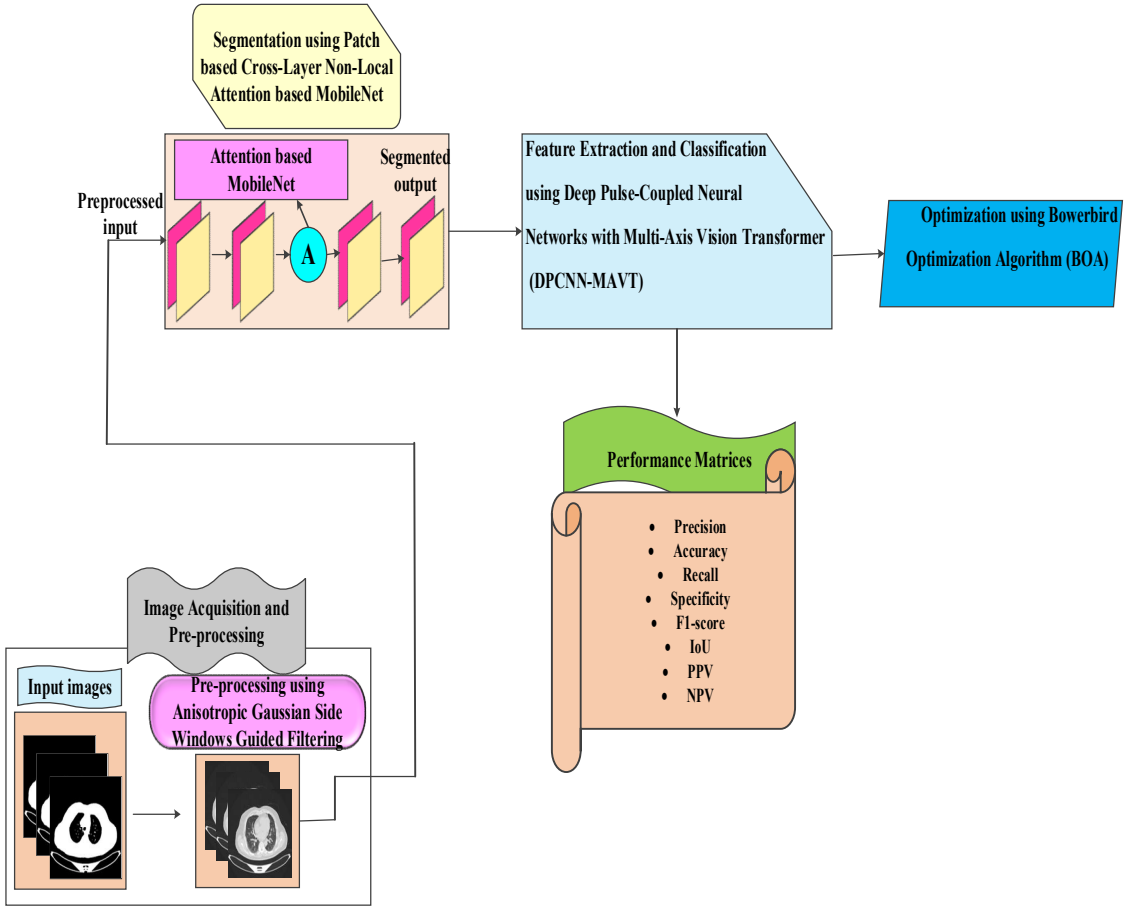

Fig 1: Workflow diagram of proposed DPCNN-MAVT-BOA method

3.1 Image Acquisition

In this input images are taken from three datasets such as LC25000 dataset, TCGA dataset and GEO dataset. These images are collected from the thermal images, so that, these images are full of noises, to remove these noises pre-processing techniques are used, they are given below:

3.2 Pre-processing using Anisotropic Gaussian Side Windows Guided Filtering (AGSWGF)

Input CT scan images are full of noise so Anisotropic Gaussian Side Windows Guided Filtering (AGSWGF) is used to remove the noises. It entails a number of steps meant to enhance the appropriateness or quality of raw photographs. AGSWGF is an advanced technique utilized in computer vision and image processing for tasks like picture augmentation and denoising. Pixels are either added or subtracted during the image scaling process. Square-sized input photos are preferable since they facilitate a more effective diagnostic process. It extends the traditional guided filtering approach by incorporating anisotropic (direction-dependent) smoothing using

Gaussian side windows. Low-pass filtering these data removes these measures entirely, but the averaging step precisely modifies the diffusion level to maintain strong edges. This procedure erodes the edge due to excessive diffusion when is large, while it preserves detail at an edge when is low due to weak diffusion. Let AGSWGF is given in equation (1):

$$R(y,x)=\delta O(y,x)+\frac{\omega_{JO}^{\mu}(y,x)}{\omega_{O}^{\mu}(y,x)^{2}+\in}\left(J(y,x)-\delta O(y,x)\right) \qquad (1)$$

where, $\delta O(y,x)$ and $\omega O(y,x)$ are as defined in the guided filtering, J is the input image, O is the guidance image, μ is the directional information range from 0 to π, $\omega_{JO}^{\mu}(y,x)$ is the cross-covariance between J and O computed using the Gaussian side window oriented at angle μ, $\omega_{O}^{\mu}(y,x)$ is the standard deviation of O within the same Gaussian side window oriented at angle μ, $\in$ is the numerical stability of a tiny positive constant.

The challenge with existing guided filters lies in their inability to fully respect the gradient variations present in the guide image, which can lead to inconsistencies in structure preservation. The covariances between input and guide patches are moderate, resulting in small influence coefficients (b_j). The averaging step rather than solely regulating (b_j) could enhance the degree of anisotropy in these filters. This approach could potentially mitigate the current shortcomings of traditional guided filter variants like AGF, WGIF, and GGIF, thereby improving their effectiveness in handling images with inconsistent structures. A weighted average strategy is given in equations (2-3):

$$\widetilde{a}_i=\sum_{i\in M(j)}q_{ji}a_i \qquad (2)$$

$$\widetilde{b}_i=\sum_{i\in M(j)}q_{ji}b_j \qquad (3)$$

where, a_i represents the value or signal at the node or pixel j, $M(j)$ denotes the neighborhood of pixel j which includes all pixels i that are considered adjacent or connected to j in some manner. q_{ji} represents the weight or coefficient associated with the connection or relationship between pixels j and i. b_j is the value or signal at the neighboring pixel i. (AGSWGF) enhances guided filtering by incorporating direction-dependent Gaussian windows. It adapts smoothing to image structures, preserving edges effectively(Fig 1).This method improves image quality by considering anisotropic characteristics of the guidance image, making it

suitable for tasks like denoising and enhancement. After that, the segmentation is applied to these previously processed images.

3.3 Segmentation using Patch based Cross-Layer Non-Local Attention based MobileNet (PCLNL- MobileNet)

After preprocessing the input images are given to the segmentation. The segmentation using MobileNet with patch-based Cross-Layer Non-Local Attention. By removing out unneeded parts, image segmentation attempts to aid the algorithm in making the best diagnosis possible. PCLNL- MobileNet refers to a technique that enhances the Mobile Net architecture with non-local attention mechanisms across different layers, focusing on patches rather than individual pixels. method reduces computational complexity without sacrificing spatial context awareness. The input feature map is given in equation (4):

$$Y \in Q^{H \times W \times C} \qquad (4)$$

where, Y denotes the tensor or array variable, Q indicates that Y contains real numbers, H is the height, W is the width, and C is the number of channels, the output feature map X with non-local attention is given in equation (5):

$$X_j = \frac{1}{D_j} \sum_i soft\max\left(g\left(Y_j, Y_i\right)\right) h\left(Y_i\right) \qquad (5)$$

where, $Y_j and\ Y_i$ are patches centered around positions j and i, g computes the affinity between patches $Y_j and\ Y_i$, h transforms Y_j, $soft$ max computes the attention weights based on the affinity scores, D_j is a normalization factor, mechanism across layers in MobileNet, each layer k computes attention over patches from previous layers is given in equation (6):

$$X_j^{(k)} = \frac{1}{D_j^{(k)}} \sum_i soft\max\left(g\left(Y_j^{(k)}, Y_i^{(k-1)}\right)\right) h\left(Y_i^{(k-1)}\right) \qquad (6)$$

where, $X_j^{(k)}$ denotes the output at position j in layer k, $D_j^{(k)}$ is the normalization factor specific to $X_j^{(k)}$, $\sum_i$ Summation over all indices i, $soft\max\left(g\left(Y_j^{(k)}, Y_i^{(k-1)}\right)\right)$ is the Softmax function applied to the affinity or similarity score $g\left(Y_j^{(k)}, Y_i^{(k-1)}\right)$ between the patch or position j in layer k and the patch or position i in layer $k-1$, $g\left(Y_j^{(k)}, Y_i^{(k-1)}\right)$ is the affinity function or score that measures the similarity or relationship between the features $Y_j^{(k)}$ at position j in layer k and

$Y_i^{(k-1)}$ at position i in layer $k-1$, $h\left(Y_i^{(k-1)}\right)$ is the transformation function applied to $Y_i^{(k-1)}$.(Eq 6)

3.4 Feature Extraction and Classification using Deep Pulse-Coupled Neural Networks with Multi-Axis Vision Transformer (DPCNN-MAVT)

After segmented the feature extraction and classification is carried out. Following processing and segmentation of the raw CT scan pictures, the images undergo an image feature extraction phase where a number of numerical features are extracted. Every pixel in a single image will yield a feature, which will subsequently be saved in a dataset. The Multi-Axis Vision Transformer (MaxViT) for further representation learning and grouping. Deep neural networks are very important in the principal domain of image classification in medical image analysis.

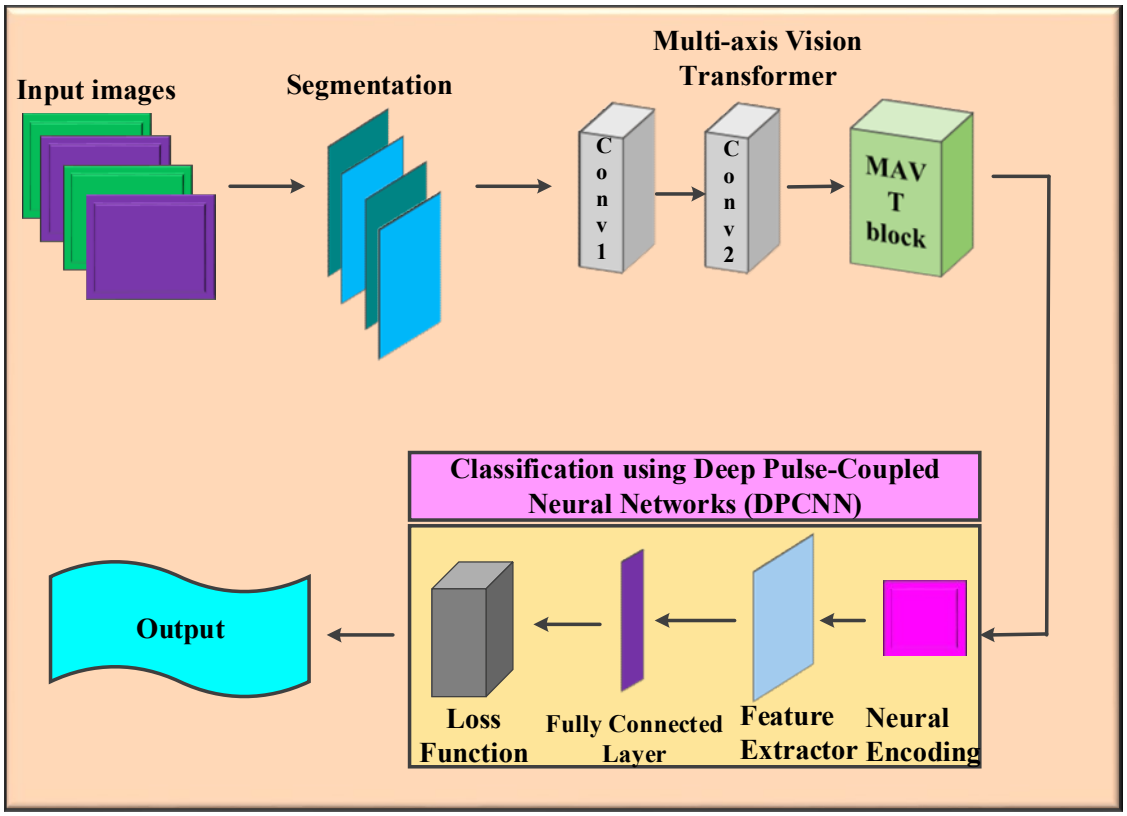

Fig 2: Architecture of Deep Pulse-Coupled Neural Networks - Multi-Axis Vision Transformer (DPCNN-MAVT)

- **Deep Pulse-Coupled Neural Networks (DPCNN)**

DPCNN is a text classification model leveraging convolutional layers with region embedding blocks to extract hierarchical features from text. Every pixel in a single image will yield a

feature, which will subsequently be saved in a dataset. A global max-pooling layer consolidates features for classification through fully connected layers, culminating in class predictions via softmax.(Fig 2) DPCNN efficiently learns hierarchical representations, excelling in tasks like sentiment analysis by effectively capturing both local and global textual dependencies. Neural encoding, feature extraction, classifier, and neural decoding are the four components that make up DPCNN.

- **Neural Encoding**

Neural encoding converts real valued inputs into spikes, involves transforming the input text into a numerical format suitable for processing by the network. Average pooling is used to prevent severe information loss that may occur with max pooling because of the banality of spikes. This could involve techniques like word embedding's or character embedding's.

- **Feature Extractor**

DPCNN uses convolutional layers to extract hierarchical features from the text. A pooling layer is used in the convolutional block to minimize feature map sizes and the location sensitivity of convolutional layers. It employs a specific type of convolutional block called the "region embedding" block. The core idea is to capture local information and gradually aggregate it to form higher-level representations is given in equation (7):

$$x_{k+1} = \omega\left(Conv\left(x_k\right) * Conv\left(x_k\right)\right) \quad (7)$$

Where, x_k represents the input feature map at layer k, $Conv(.)$ denotes a convolution operation followed by a non-linear activation, $*$ denotes the max-pooling operation over a fixed-size window, ω represents the activation function applied element-wise to the result of the convolution operation $Conv\left(x_k\right) * Conv\left(x_k\right)$, x_{k+1} represents the output of the $k-1$-th layer in the neural network.

- **Classifier (Fully Connected Layers)**

Classifying the retrieved features is subsequently done using a fully connected layer classifier. A global max-pooling operation is carried out following multiple layers of region embedding blocks to produce a fixed-size representation of the complete text. To forecast the probabilities for each class in a classification job, this pooled representation is then fed into fully connected layers and softmax activation is applied after that.

- **Loss Function**

The DPCNN's loss function is the temporal efficient training cross-entropy, which can help to increase performance and smooth the loss landscape is given in equation (8):

$$K = \frac{1}{S}\sum_{s=1}^{S} K_{BF}\left(soft\max\left(P^{s}\right), x\right)$$

$$K = \frac{1}{S}\sum_{s=1}^{S} K_{BF}\left(\widetilde{P}^{t}, x\right) \qquad (8)$$

$$K = -\frac{1}{S}\sum_{s=1}^{S}\sum_{j} x_{j} \log \widetilde{P}_{j}^{s}$$

where, K_{BF} signifies loss of cross-entropy, x indicates the target label's single hot coding., P^{s} shows the synaptic current at a given time step, s of the output non linking DPCNN, the softmax function modifies P^{s} into a vector of probability $\widetilde{P}^{t}$, x_{j} is the true label or target distribution corresponding to time step j, S is the number of time steps or sequence length over which the loss is averaged.

Step1: Initialization

Generate an initial population of Snow geese (possible solutions), with each representing a DPCNN-MAVT set of hyper parameters.

Step 2: Random Generation

Randomly generate the optimization parameters of Bowerbirds to attain the best solution.

Step 3: Fitness function

The fitness function is used to predict the objective function, which is to correctly classify the malignant and non-cancerous zones. It is given in equation (11):

$$Fitness\ Function = Minimize\left(\sigma\right), Maximize\left(W\right) \qquad (11)$$

where, σ is used for reducing error rate, processing time, computational complexity and cost, W is used to improve accuracy.

Step 4: Elitism (Exploration) for improving accuracy

Elitism is a mechanism commonly used in evolutionary algorithms, including met heuristic algorithms like the Bowerbird Optimization Algorithm (BOA), to ensure that the best solutions discovered so far are preserved across generations. It promotes the retention of high-quality solutions (also known as elites) from one generation to the next, preventing the algorithm from losing its best solutions due to the randomness of mutation or crossover operations is given in equation (12):

$$Y^{(s)} = \left\{ y_j^{(s)} \right\}_{j=1}^{M} \qquad (12)$$

where, s represents the current iteration or generation of the algorithm, $Y^{(s)}$ is the entire set of the solutions considered by the algorithm at iteration s, j is the index indicating the position of the solution within the population $Y^{(s)}$, $y_j^{(s)}$ is the j - th solution in the population $Y^{(s)}$ at iteration s, $\left\{ y_j^{(s)} \right\}_{j=1}^{M}$ denotes the collection of all M solutions $y_j^{(s)}$ within the population $Y^{(s)}$.

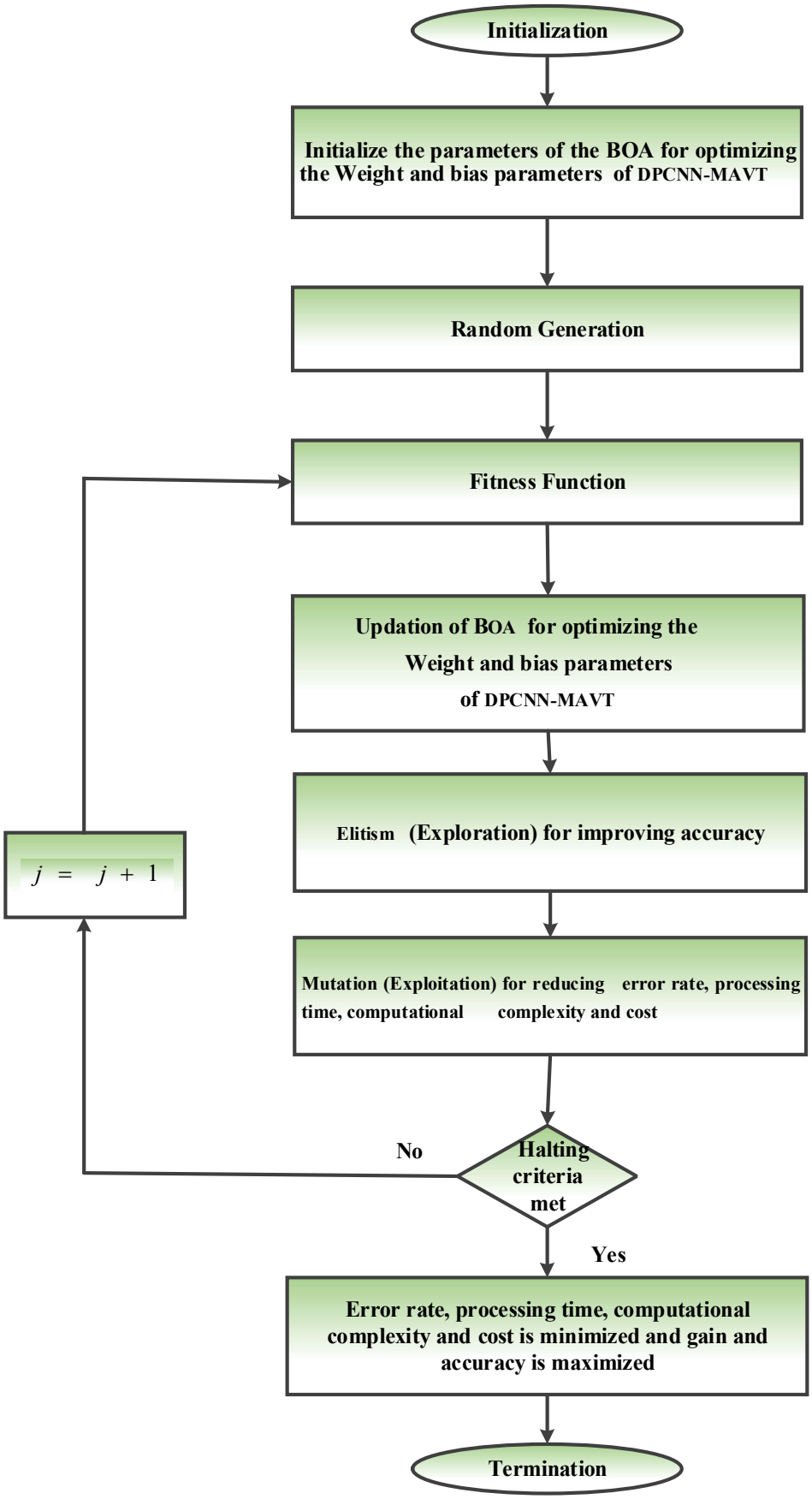
Initialization
Initialize the parameters of the BOA for optimizing the Weight and bias parameters of DPCNN-MAVT
Random Generation
Fitness Function
Updation of BOA for optimizing the Weight and bias parameters of DPCNN-MAVT
Elitism (Exploration) for improving accuracy
Mutation (Exploitation) for reducing error rate, processing time, computational complexity and cost
Halting criteria met
No
Yes
j = j + 1
Error rate, processing time, computational complexity and cost is minimized and gain and accuracy is maximized
Termination

Fig 3: Flow chart of BOA

Step 5: Mutation (exploitation) for reducing error rate, processing time, computational complexity and cost

Males who are engaged in constructing a ground-level bower run the risk of being attacked by other animals or receiving no attention at all. At the conclusion of every algorithmic cycle, random modifications are implemented with a specific likelihood(Fig 3). Mutation typically involves randomly modifying one or more components (genes) of a solution to explore neighboring solutions that may not be directly reachable through crossover or other operation is given in equation (13):

$$y_{jl}^{new} \sim M\left(y_{jk}^{old}, \mu^2\right) \qquad (13)$$

where, y represents a variable, *new* denote something new or different, jl be a subscript or an index, $\sim$ symbol usually means negation, $M(y)$ be a function or predicate involving y, μ^2 denote variance.

The value of μ is proportional to the space width is given in equation (14):

$$\mu = x \times \left(\text{var}_{\max} - \text{var}_{\min}\right) \qquad (14)$$

where, μ represents the standard deviation or possibly another measure of dispersion, x coefficient or factor that scales the difference between $\text{var}_{\min}$ and $\text{var}_{\max}$, $\text{var}_{\max}$ denotes the maximum value or upper limit of some variable, $\text{var}_{\min}$ denotes the minimum value or lower limit of the same variable.

Step 6: Termination

Once the best answers are obtained using equations (11–13), end the operation. Additionally, equation (11) yields the most accurate answer, whereas equation (13) minimizes error rates, processing times, computing complexity, and cost. This iteration is continuing until the halting criteria $j = j + 1$ is met. Finally, the proposed DPCNN-MAVT-BOA accurately classifies the Non-Small Cell lung Cancer as normal and Tumor. (Fig 3)

4. Result and Discussions

This section describes the introduced scheme's findings and debate. Python is used to carry out the Result and discussion of the method. Here is some of the Implementation parameter is mentioned in table 2:

Table 2: Implementation Parameters

Parameters	Description
Proposed Neural Network	DPCNN-MAVT-BOA
OS	Windows 10
Optimization	BOA
Dataset	LC25000 dataset, TCGA dataset and GEO dataset
Software	Python 3.7
Epoches	3000

4.1 Dataset Description

To classify the NSCLC, three NSCLC datasets are taken; they are LC25000 dataset, TCGA dataset and GEO datasets its descriptions are given below:

4.1.1 LC25000 dataset [16]

Five thousand pictures of every kind of lung and colon cancer can be found in the LC25000 collection. The dataset satisfies HIPAA regulations and has been verified. There were only 750 original photographs collected in all, 250 of which were assigned to each category and measured 1024 x 768 pixels. Python is used to reduce the size of these photos to 768x768 pixels, and the software program augmenter is used to increase their size. The LC25000 dataset contains two classes namely benign and malignant.

4.1.2 TCGA dataset [20]

Using the TCGA training dataset (n=62), the tumor regions were identified from each layer of the CT scans of the NSCLC patients.The tumor areas were first manually drawn using 3D Slicer software, and then they were rebuilt in three dimensions. There were 1037 unique radiomics features found in the tumor simulation photos. From these 1037 radiomics features,

six major categories were found: first-order, gray level run-length matrix (GLRLM), gray level size zone matrix (GLSZM), gray level co-occurrence matrix (GLCM), neighborhood gray tone difference matrix (NGTDM), and gray level dependence matrix (GLDM). It is further divided into two classes namely, tumor and normal.

4.1.3 GEO dataset [25]

There were 151 healthy human participants in this dataset when they signed up for the research. After enrollment, each person received a virus, H1N1, H3N2, HRV, or RSV are the four types. Patterns of gene expression in both infected and uninfected people were obtained by taking blood samples from them at certain intervals, including prior to inoculation. They are further divided into two classes namely, tumor and normal.

4.2 Performance metrics:

The Performance measures such Precision, f1-score, recall, accuracy, Intersection Over Union, specificity, Jaccard index, Dice coefficient, error rate and analysis of proposed algorithm are analyzed the proposed DPCNN-MAVT-BOA method's efficiency is contrasted with a number of current techniques, including CNN [16], MorphAttnNet [17] K-NN [18] PJGC-Net [19] in LC25000 dataset WGCN [20] PPIN [21] FFNN [22] 3D Slicer [23] in TCGA dataset and WGCN [20] PCM1 [24] LOADDx [25] SCADDx [26] in GEO dataset respectively and Table 3 shows the performance metrics and equation. The performance metrics equations are given below:

True positive $\alpha\varphi$: Normal accurately forecasts as normal.

False positive $\alpha\phi$: The false positive misclassifies normal as abnormal.

False negative $\beta\varphi$: The false negative misconstrues an aberrant situation as being common in an unusual way.

True negative $\beta\phi$: Remarkably precise predictions of unnatural.

Intersection over Union (IoU): A statistical measure used to assess the accuracy of an item detector on a certain dataset.

Positive Predictive Value (PPV): The measure of how someone who tests positive for a disease is known as the positive predictive value.

Negative predictive value (NPV): The NPV is defined as the proportion of true negative results in all negative tests. It measures how often a person who tests negative truly does not

have the disease. NPV is calculated by dividing the number of true negatives (TN) by the sum of true negatives (TN) and false negatives (FN).

Table 3 Performance Metrics

Performance metrics	Equation
Precision	$\frac{\alpha\varphi}{\alpha\varphi + \alpha\phi}$
Accuracy	$\frac{\alpha\varphi + \beta\phi}{\alpha\varphi + \beta\phi + \alpha\phi + \beta\varphi}$
Recall	$\frac{\alpha\varphi}{\alpha\varphi + \beta\varphi}$
Specificity	$\frac{\beta\phi}{\beta\phi + \alpha\phi}$
F1-score	$2.\frac{p \cdot r}{p + r}$
IoU	$\left(\frac{Overlap\,Area}{Union\,Area}\right)$
PPV	$\frac{\alpha\varphi}{\alpha\varphi + \alpha\phi}$
NPV	$\frac{\beta\phi}{\beta\phi + \beta\varphi}$

where, *Overlap Area* represents the segment connecting the ground-truth area with the anticipated area and *Union Area* represents the area that is included in the predicted area and the ground-truth area, p represents the precision, r represents the recall.(Table 3)

4.3 Performance Analysis:

In this section, the performance analysis of the proposed method is related with existing methods. Positive predictive value, negative predictive value, f1-score, IoU, recall, accuracy, and specificity. The efficiency of the proposed DPCNN-MAVT-BOA method is examined using the proposed algorithm in comparison to some existing methods, including CNN [16], MorphAttnNet [17], K-NN [18], PJGC-Net [19] in the LC25000 dataset, WGCN [20] PPIN [21] FFNN [22], 3D Slicer [23] in the TCGA dataset, and WGCN [20] PCM1 [24] LOADDx [25] SCADDx [26] in the GEO dataset, respectively.

4.3.1 Estimation of performance of the proposed approach:

The performance analysis of the proposed method is clarified in this section. The figure 4 shows the output results of LC25000 dataset with 2 classes such as benign and malignant.

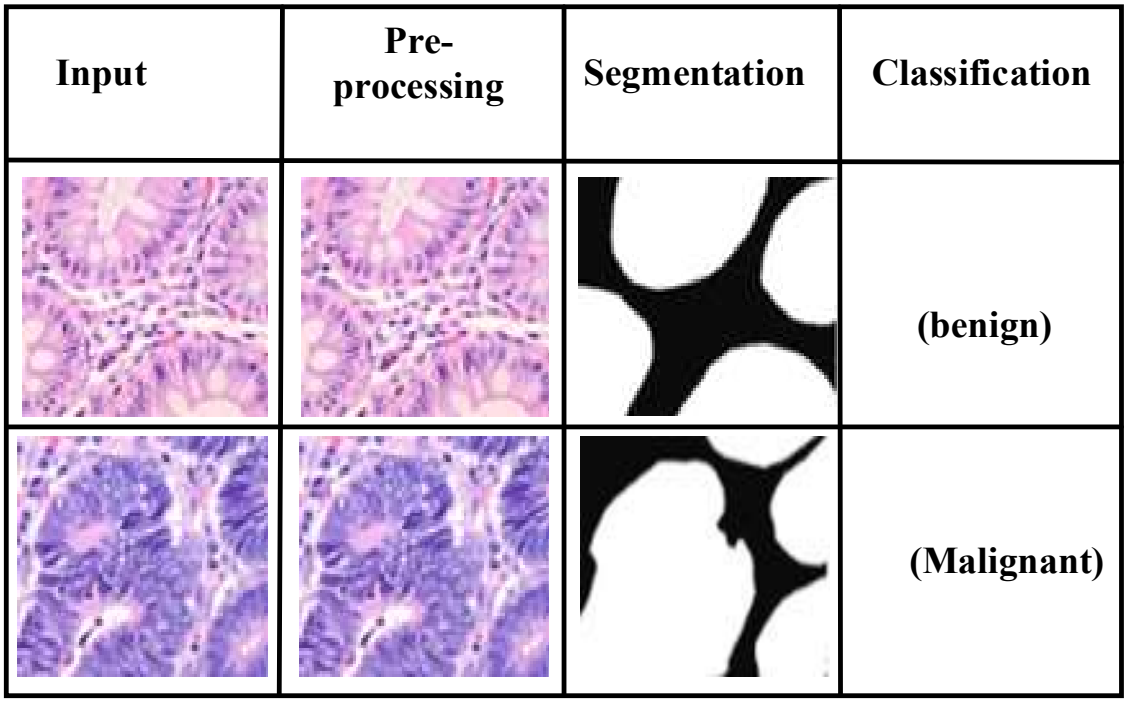

Fig 4: Output results of LC25000 dataset

The figure 5 shows the output results of TCGA dataset, which contains 2 Classes such as, two classes namely, tumor and normal.

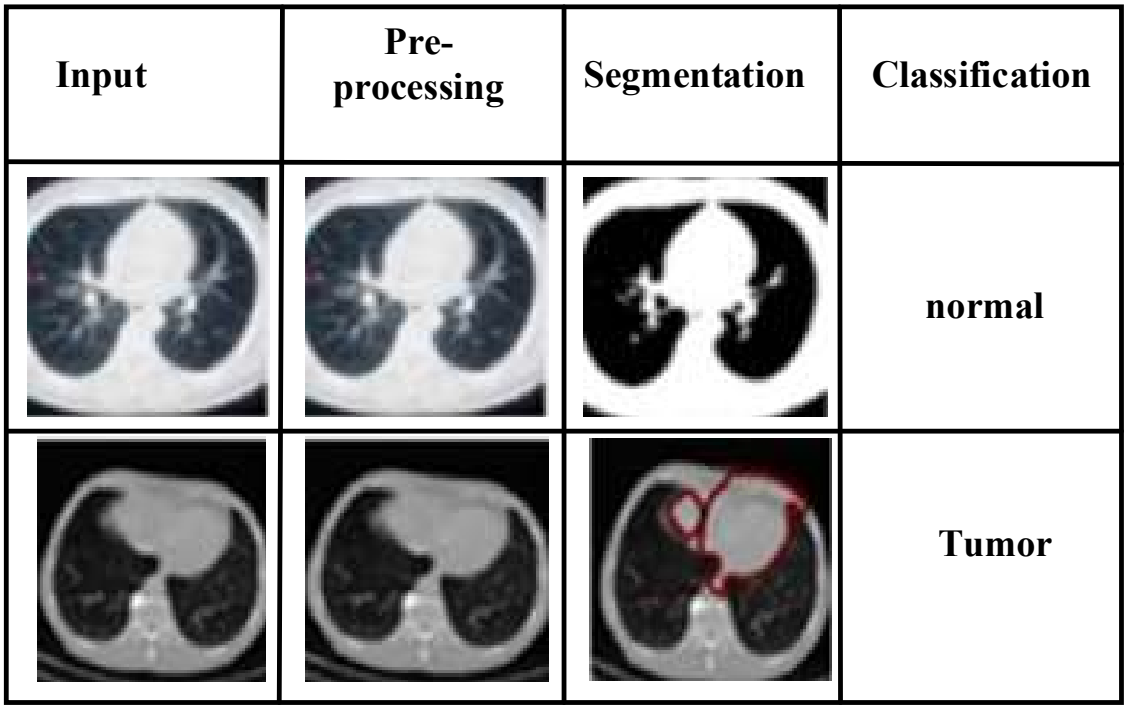

Fig 5: Output results of TCGA dataset

The figure 6 shows the output results of GEO dataset, which contains 2 Classes such as, two classes namely, tumor and normal.

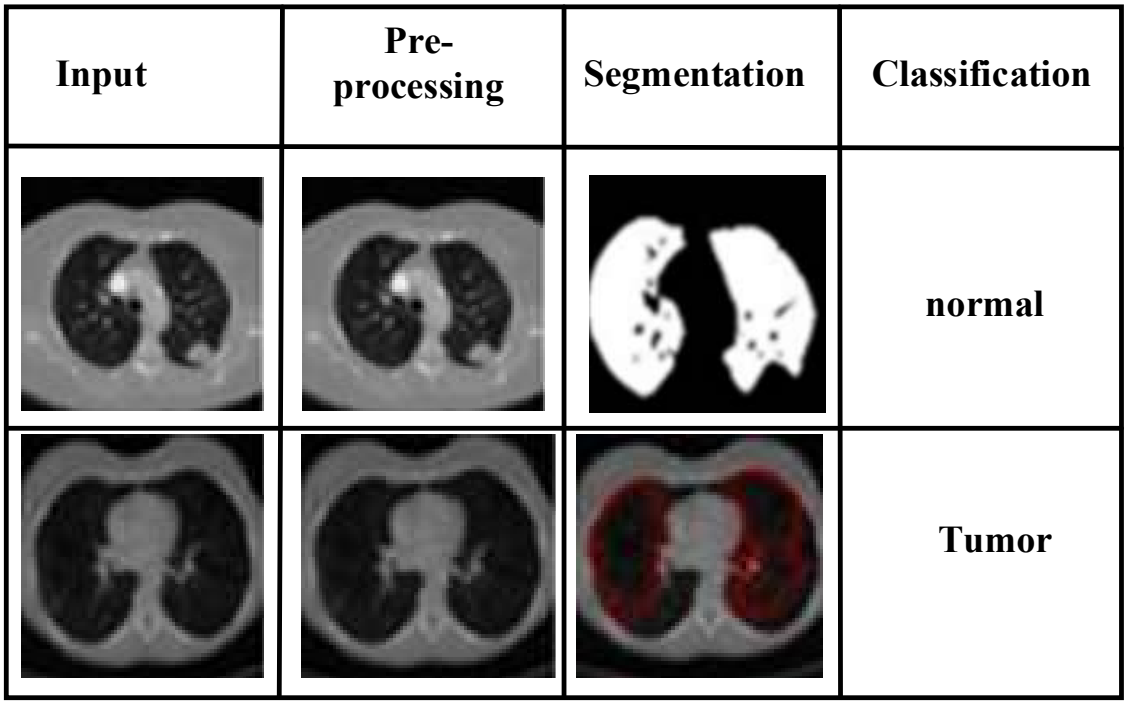

Fig 6: Output results of GEO dataset

Fig 7: Accuracy, specificity, F1-score for (a) LC25000 dataset, (b) TCGA dataset, (c) GEO dataset

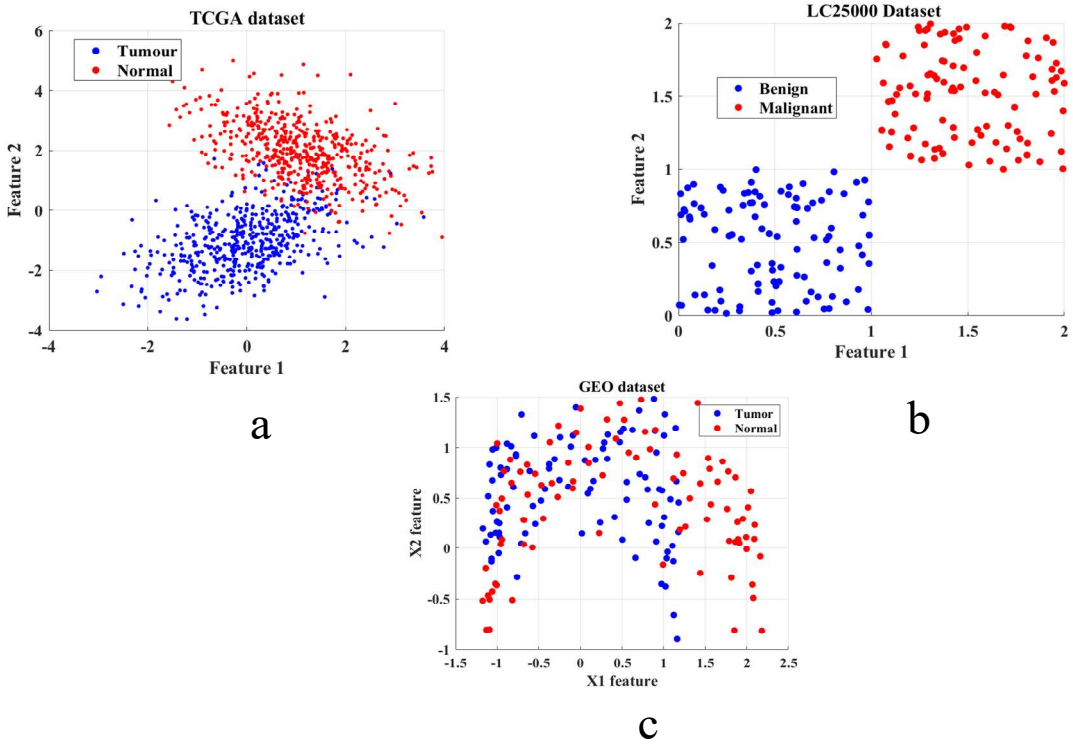

Figure 7 shows Precision, f1-score, recall, accuracy, Intersection Over Union, specificity, PPV,NPV and error rate analysis for LC25000 dataset, TCGA dataset and GEO datasets and the proposed method is compared with existing methods such as CNN[16], MorphAttnNet[17] K-NN[18] PJGC-Net[19] in LC25000 dataset WGCN[20] PPIN[21] FFNN[22] 3D Slicer[23] in TCGA dataset and WGCN [20] PCM1[24] LOADDx [25] SCADDx[26] in GEO dataset respectively. The accuracy of proposed method attains 99.78%, whereas the existing method attains 87.52%, 84.50%, 87.35% and 95.76% respectively for 3 datasets.

Fig 8: (a) Training Accuracy for (a) LC25000 dataset, (b) TCGA dataset, (c) GEO dataset

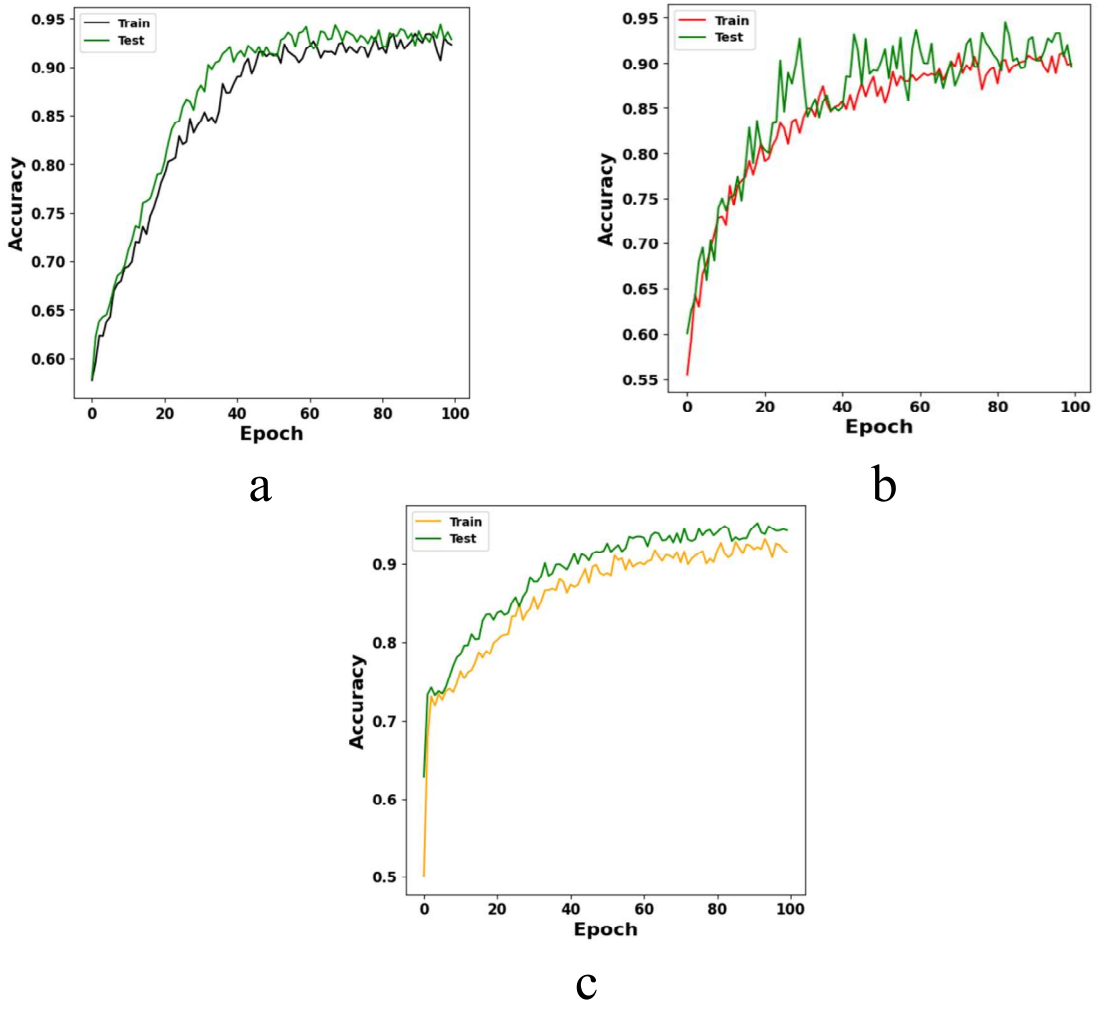

Figure 8 shows the performance analysis of Training Accuracy for (a) LC25000 dataset, (b) TCGA dataset, (c) GEO dataset with 99.78% accuracy. By evaluating the model's performance on the training set, training accuracy offers valuable information about how well the model is assimilating the material it has encountered. (Fig 8)

Figure 9 shows the Loss function for (a) LC25000 dataset, (b) TCGA dataset, (c) GEO dataset. One important measure of the model's learning efficiency during training is the loss function. A lower loss function value indicates greater model performance.

Figure 10 shows the ROC curves for the 3 datasets such as LC25000 dataset, TCGA dataset and GEO datasets and the proposed method is compared with existing methods such as CNN [16], MorphAttnNet [17], K-NN [18], PJGC-Net [19] in LC25000 dataset WGCN [20] PPIN[21] FFNN [22] 3D Slicer[23] in TCGA dataset and WGCN [20] PCM1[24] LOADDx [25] SCADDx[26] in GEO dataset correspondingly. A graphical representation called a Receiver Operating Characteristic (ROC) curve shows how well a binary classifier system can diagnose problems as its discrimination threshold is changed(Fig 10)

Table 4: Comparison of Accuracy, Precision, Specificity, Recall, IoU, PPV, NPV and Error sets.

Datasets	**Methods**	**Acc (%)**	**Pre (%)**	**Spe (%)**	**Recall (%)**	**IoU (%)**	**PPV (%)**	**NPV (%)**	**Error (%)**
LC25000 dataset	CNN [16]	87.61	98.5	96.88	96.4	96.77	97.3	89.34	0.5
LC25000 dataset	MorphAttnNet [17]	87.52	76.7	87.9	83.6	90.24	88.6	92.15	0.7
LC25000 dataset	K-NN [18]	86.73	89.6	89.97	89.11	90.23	91.72	92.66	0.4
LC25000 dataset	PJGC-Net [19]	88.69	87.5	86.68	86.68	93.51	89.97	94.29	0.4
TCGA Dataset, GEO dataset	WGCN [20]	84.50	91.4	88.4	87.5	91.29	87.4	93.49	0.5
TCGA dataset	PPIN [21]	95.97	99.7	99.7	99.28	99.65	99.47	96.29	0.9

TCGA dataset	FFNN [22]	97.37	89.3	95.1	98.5	86.26	97.43	88.75	0.2
TCGA dataset	3D Slicer [23]	96.52	84.9	92.4	83.9	91.27	94.31	91.24	0.3
GEO dataset	PCM1 [24]	96.45	93.23	78.23	92.34	93.67	94.52	86.25	0.6
GEO dataset	LOADDx [25]	87.35	95.56	94.67	86.67	87.67	90.56	89.37	0.8
GEO dataset	SCADDx [26]	83.39	86.45	89.45	93.34	82.22	84.90	93.45	0.9
LC25000, TCGA and GEO dataset	**DPCNN-MAVT-BOA (proposed)**	**99.78**	**96.35**	**99.34**	**97.29**	**98.47**	**96.78**	**91.34**	**0.1**

In this section Acc represents accuracy, pre represents the precision, spe represents the specificity, IoU represents the intersection over union, PPV represents the positive predictive value and NPV represents the Negative Predictive Value.

Table 4 compares the proposed method to existing methods such as CNN [16], MorphAttnNet [17] K-NN [18] PJGC-Net [19] in LC25000 dataset WGCN [20] PPIN [21] FFNN [22] 3D Slicer [23] in TCGA dataset and WGCN [20] PCM1 [24] LOADDx [25] SCADDx [26] in GEO dataset respectively. The proposed technique achieves the best accuracy (99.2%), precision (96.3%), Spe (99.34%), Recall (97.29%), IoU (98.47%), ppv (96.78) and NPV (9134). It also confirms the shortest processing time (0.1) and error rate (0.1) indicating its efficiency and dependability.(Table 4)

Table 5. **Average classifier outcome of DPCNN-MAVT-BOA under varying epochs.**

Avg values (%)							
No of epoches	**Accuracy (%)**	**Precision (%)**	**Specificity (%)**	**Recall (%)**	**IoU (%)**	**Ppv (%)**	**NPV (%)**
250	87.61	98.5	96.88	96.4	96.77	97.3	89.34
500	87.52	76.7	87.9	83.6	90.24	88.6	92.15
750	86.73	89.6	89.97	89.11	90.23	91.72	92.66
1000	88.69	87.5	86.68	86.68	93.51	89.97	94.29
1250	84.50	91.4	88.4	87.5	91.29	87.4	93.49
1500	95.97	99.7	99.7	99.28	99.65	99.47	96.29

4.5 Ablation study of the proposed method

An ablation study is a methodical experiment carried out to examine the effects of specific elements or characteristics of a suggested approach(Table 5). An ablation study for the suggested method DPCNN-MAVT-BOA would include methodically eliminating or adjusting particular elements or methods in order to determine how they affect the model's overall performance. Table 6 demonstrates the ablation study of the projected method compared with previous Attention networks.

Table 6: Ablation study

Methods	LC25000 dataset	TCGA dataset	GEO dataset
Performance metrics	**Accuracy (%)**	**Accuracy (%)**	**Accuracy (%)**
Attention with DCNN-MAVT	87.61	95.97	87.37
Attention with BOA	87.52	84.50	87.35
Attention with DPCNN-MAVT-BOA	**99.78**	**99.78**	**99.78**

From table 6 comparisons of altered configurations of the model and their performance on 3 datasets. The proposed method attains better results by adding Attention with MAVT and Deep Pulse-Coupled Neural Network. Without these networks this method attains less accuracy. The configuration Attention with CNN exhibits a slight drop in accuracy and attains 87.61% for first dataset, 95.97% for second dataset and 87.37% for third dataset. Similarly, the variant Attention with BOA shows a slight increase from Attention with DCNN, with accuracy 99.78% for three datasets. Hence, the proposed Attention with DPCNN-MAVT+BOA attains the accuracy of 99.78%for three datasets respectively.

5. Conclusion

In this manuscript, the input data is taken from three dataset such as LC25000, TCGA and GEO dataset. Then these data are pre-processed using AGSWGF method. Following that, NSCLC is segmented using the PCLNL- MobileNet. Then the Feature Extraction and classification are done using DPCNN-MAVT for detecting the normal and tumor NSCLC. The introduced system is executed in python. The efficiency of the proposed DPCNN-MAVT-BOA is analyzed using 3 datasets and attains 99.78% accuracy and 0.1% error rate, compared with the existing methods. This indicates the approach's superior efficiency and potential for further development in the field. Future work will enhance model robustness and generalizability by expanding dataset, integrating real-time processing, and creating a user-friendly interface for detecting the NSCLC.

References:

1. Demiroğlu, Uğur, et al. "Classification of computerized tomography images to diagnose non-small cell lung cancer using a hybrid model." *Multimedia Tools and Applications* 82.21 (2023): 33379-33400.
2. Lin, Jing, et al. "Classification of histological types and stages in non-small cell lung cancer using radiomic features based on CT images." *Journal of digital imaging* 36.3 (2023): 1029-1037.
3. Atiya, Shaik Ummay, N. V. K. Ramesh, and B. Naresh Kumar Reddy. "Classification of non-small cell lung cancers using deep convolutional neural networks." Multimedia Tools and Applications 83.5 (2024): 13261-13290.
4. Helaly, Hadeer A., et al. "ELCD-NSC2: a novel early lung cancer detection and non-small cell classification framework." Neural Computing and Applications (2024): 1-16.
5. Zhao, Hongyue, et al. "Non-invasively discriminating the pathological subtypes of non-small cell lung cancer with pretreatment 18F-FDG PET/CT using deep learning." Academic Radiology 31.1 (2024): 35-45.
6. Tomassini, Selene, et al. "On-cloud decision-support system for non-small cell lung cancer histology characterization from thorax computed tomography scans." Computerized Medical Imaging and Graphics 110 (2023): 102310.
7. Wang, Jiexiao, et al. "CT radiomics-based model for predicting TMB and immunotherapy response in non-small cell lung cancer." BMC Medical Imaging 24.1 (2024): 45.
8. Dora, David, et al. "Computed Tomography-Based Quantitative Texture Analysis and Gut Microbial Community Signatures Predict Survival in Non-Small Cell Lung Cancer." Cancers 15.20 (2023): 5091.
9. Zhu, Min, et al. "Newly diagnosed non-small cell lung cancer with interstitial lung abnormality: prevalence, characteristics, and prognosis." Thoracic Cancer 14.19 (2023): 1874-1882.
10. Pasini, Giovanni, et al. "Phenotyping the histopathological subtypes of non-small-cell lung carcinoma: how beneficial is radiomics?." Diagnostics 13.6 (2023): 1167.
11. Shevtsov, Alexey E., et al. "Evaluating the Potential of Metastatic Mediastinal Lymph Node Involvement in Non-Small Cell Lung Cancer Patients through Convolutional Neural Networks Analysis of Chest CT." medRxiv (2024): 2024-05.

12. Chakrabarty, N., et al. "Imaging of brain metastasis in non-small-cell lung cancer: indications, protocols, diagnosis, post-therapy imaging, and implications regarding management." Clinical Radiology 78.3 (2023): 175-186.
13. Yoo, Jang, et al. "Radiomics Analysis of 18F-FDG PET/CT for Prognosis Prediction in Patients with Stage III Non-Small Cell Lung Cancer Undergoing Neoadjuvant Chemoradiation Therapy Followed by Surgery." Cancers 15.7 (2023): 2012.
14. Ragab, Mahmoud, et al. "Self-Upgraded Cat Mouse Optimizer with Machine Learning Driven Lung Cancer Classification on Computed Tomography Imaging." IEEE Access (2023).